International Journal of Non-Linear Mechanics 47 (2012) 135–143

Contents lists available at ScienceDirect

International Journal of Non-Linear Mechanics

journal homepage: www.elsevier.com/locate/nlm

On the bifurcations of the Lamé solutions in plane-strain elasticity ☆

Ciprian D. Coman *, Xiang Liu

University of Glasgow, School of Mathematics and Statistics, 15 University Gardens, Glasgow G12 8QW, Scotland

ARTICLE INFO

Available online 2 April 2011

Keywords:
Incremental elasticity
Singular perturbations
Loss of ellipticity
Surface instability

ABSTRACT

We consider the in-plane bifurcations experienced by the Lamé solutions corresponding to an elastic annulus subjected to radial tension on the curved boundaries. Numerical investigations of the relevant incremental problem reveal two main bifurcation modes: a long-wave local deformation around the central hole of the domain, or a material wrinkling-type instability along the same boundary. Strictly speaking, the latter scenario is related to the violation of the Shapiro–Lopatinskij condition in an appropriate traction boundary-value problem. It is further shown that the main features of this material instability mode can be found by using a singular-perturbation strategy.

1. Introduction

Elastic instabilities of bulky solids and thick-walled structural elements, such as plates and shells, have received considerable attention for the past several decades, starting with the works of Biot on incremental elasticity in the 1930s, which were later collected in [1]. A more modern treatment, together with many interesting examples, can be found in the classic text by Ogden [2].

While for most part there is a close parallel between the bifurcations experienced by thin-walled bodies modelled with the help of classical plate and shell theories, on the one hand, and those of three-dimensional elastic bodies, on the other, a number of complementary issues arise in the latter situation. Largely speaking, these are related to the possible loss of ellipticity in the incremental bifurcation equations and the existence of surface instabilities [3,4]; this last phenomenon is typical of compressed half-planes or half-spaces and has no counterpart in the classical theories of buckling. It is precisely these two aspects, and related phenomena, that we wish to revisit here within the scope of an approximate set of incremental bifurcation equations described by Novozhilov in his book [5]; this model can be traced back to some early incremental equations proposed by Biezeno and Hencky [6] as well as Biot ([1], pp. 490–491). For convenience we shall refer to this model as the *simplified incremental deformation theory* (SIDT for short). To a certain extent, these incremental models are superior to the buckling equations used in structural mechanics, reason for which in recent years they have been the object of several quantitative studies (e.g., [7–10]). The mathematical structure of these equations in the case of non-homogeneous stress fields appears to be little explored and, as seen in what follows, deserves much more consideration.

In some recent work [11] the first author and M. Destrade have investigated the asymptotic structure of the instability experienced by an incompressible neo-Hookean rubber block subjected to pure flexure (see [12] for some experimental considerations on the same problem). Based on the exact non-linear pre-bifurcation solution obtained by Rivlin in [13] it was found that if the ratio of thickness to length was κ then for $0<\kappa<\infty$ the bent block displayed an Euler-type instability with a well-defined number of ripples on the compressed side, but in the limit $\kappa\to\infty$ this degenerated into a kinematic surface instability. In a later study [14] it was shown that the turning points found in the differential equation associated with the pure bending problem played only a passive role, in contrast to a deceivingly similar situation that crops up in relation to the wrinkling of stretched thin films [15,16]—where turning points did play a crucial role.

The above instability scenario was associated with one of the traction-free circular surfaces of the bent block (the one that was in compression); the eversion of a cylindrical thick-walled tube represents an akin situation amenable to the same type of asymptotic treatment, as demonstrated by the first author [18]. A question that still remains is whether the asymptotic strategy developed in these studies can find any applicability to the case when the bifurcation is associated with a stressed rather than a free surface.

The problem we have in mind is that of a long hollow cylindrical body subjected to radial tensions on both boundaries. Invoking the standard plane-strain simplifications we can confine our attention to cross-sections situated sufficiently far away from the two ends of the cylinder. Thus, we are essentially dealing with a two-dimensional problem and a number of further simplifications can be called upon. For instance, if we assume that the pre-bifurcation state is sufficiently weak, so that linear elasticity is applicable, then the expressions of the stress and displacement fields are given by the

☆ Dedicated with esteem and admiration to Professor Ray Ogden, F.R.S., on the occasion of his award of the Prager Medal 2010.

* Corresponding author.
E-mail address: Ciprian.Coman@glasgow.ac.uk (C.D. Coman).

0020-7462/$ - see front matter © 2011 Elsevier Ltd. All rights reserved.
doi:10.1016/j.ijnonlinmec.2011.03.015

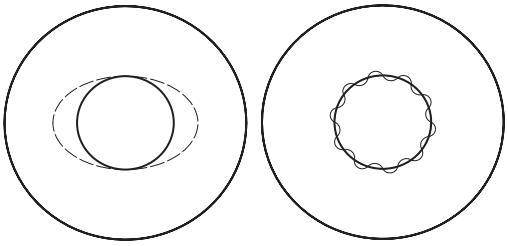

Fig. 1. Long- and short-wavelength local deformations of the annulus.

Lamé solution for a radially loaded annulus (e.g., see [19]). It is a well-known fact that for tensile loads this solution predicts a typical stress concentration around the perimeter of the inner hole, so we expect the possible bifurcations to have a local character. However, it is not at all obvious *a priori* whether the inner rim will prefer a long-wave deformation mode, as seen in the left sketch in Fig. 1, or whether it will have the tendency to accumulate many ripples (right sketch, same Figure). Of course, a third possibility is material failure as heralded by loss of ellipticity prior to any changes in the radially symmetric pre-bifurcation state. All these questions will be addressed in the subsequent parts of the paper.

As already hinted above, the SIDT has attracted interest in recent time, particularly in relation to buckling of thick circular cylindrical shells under hydrostatic pressure. Kardomateas and his associates have explored such aspects extensively (e.g., [7,8] and the references therein). While not entirely as accurate as the incremental equations found in [1] or [2], they represent a versatile alternative whose status is perhaps somewhere between classical plate/shell models and those found in the last two references just cited.

The paper is laid out as follows. In Section 2 we review the SIDT by presenting an intrinsic-form derivation of the relevant equations; a brief glancing at the equivalent traditional-notation calculations ("á la Timoshenko") that appear in [7] indicates clearly the advantages of the route pursued here. We also take this opportunity to record in Section 2 one of the possible extensions of these equations, whose detailed analysis will be reported elsewhere. By using the normal-mode approach, the bifurcation equations are reduced to an eigenvalue problem for two coupled second-order ordinary differential equations with variable coefficients. Direct numerical simulations are then employed in Section 3 to investigate the character of the possible linear bifurcations. This aspect turns out to be sensitive to the type of traction boundary conditions imposed on the curved boundaries of the annulus. Two complementary cases are discussed: (i) *dead loads* (i.e. the outward unit normal to the boundary remains unchanged in passing from the stressed configuration to the neutrally stable one), and (ii) *follower loads* (assumed to follow the direction of the normal to the boundary). As it happens, the outcome in both cases turns out to be somewhat similar, in the sense that the predominant instability mode is the short-wavelength deformation pattern seen on the right-hand side in Fig. 1. Strictly speaking, the number of ripples along the inner rim is infinite and the "bifurcation" is linked with the failure of the *Shapiro–Lopatinskij Condition* (SLC) in the corresponding incremental traction boundary-value problem—e.g., see [21] (pp. 106–108). The recent paper [22] contains a number of interesting discussions in the context of non-linear elasticity problems and abstract bifurcation theory, as well as an extensive list of references. Motivated by our numerical findings, in Section 4 we indicate how some of the quantitative aspects of this material instability can be understood by a simple boundary-layer argument involving the mode number as the main asymptotic parameter.

Before we embark on our analysis, a word about the non-standard notation that will appear below is in order. With $\mathrm{GT}(n)$ standing for the set of all general tensors of order n, we define two partial transposition operations for elements of $\mathrm{GT}(3)$, $(\,)^t$ and ${}^t(\,)$, according to the following rules: $(\boldsymbol{a}\otimes\boldsymbol{b}\otimes\boldsymbol{c})^t\cdot\boldsymbol{x}\equiv(\boldsymbol{a}\otimes\boldsymbol{c}\otimes\boldsymbol{b})\cdot\boldsymbol{x}=\boldsymbol{a}\otimes\boldsymbol{c}(\boldsymbol{b}\bullet\boldsymbol{x})$ and ${}^t(\boldsymbol{a}\otimes\boldsymbol{b}\otimes\boldsymbol{c})\cdot\boldsymbol{x}\equiv(\boldsymbol{b}\otimes\boldsymbol{a}\otimes\boldsymbol{c})\cdot\boldsymbol{x}=\boldsymbol{b}\otimes\boldsymbol{a}(\boldsymbol{c}\bullet\boldsymbol{x})$ for all $\boldsymbol{x}\in\mathrm{GT}(1)$; here "$\bullet$" denotes the scalar product of two vectors and "$\cdot$" represents the simple contraction between elements of various $\mathrm{GT}(n)$ and $\mathrm{GT}(m)$, $m+n>2$. We also use two other different types of contractions: the double contraction ":" between various tensors is taken as $(\boldsymbol{a}\otimes\boldsymbol{b}):(\boldsymbol{c}\otimes\boldsymbol{d})\equiv(\boldsymbol{a}\bullet\boldsymbol{c})(\boldsymbol{b}\bullet\boldsymbol{d})$, $(\boldsymbol{a}\otimes\boldsymbol{b}):(\boldsymbol{c}\otimes\boldsymbol{d}\otimes\boldsymbol{e})\equiv(\boldsymbol{a}\bullet\boldsymbol{c})(\boldsymbol{b}\bullet\boldsymbol{d})\boldsymbol{e}$, etc, and the triple contraction between third- and fourth-order tensors, "$\vdots$" which obeys the rule $(\boldsymbol{a}\otimes\boldsymbol{b}\otimes\boldsymbol{c})\vdots(\boldsymbol{d}\otimes\boldsymbol{e}\otimes\boldsymbol{f}\otimes\boldsymbol{g})\equiv(\boldsymbol{a}\bullet\boldsymbol{d})(\boldsymbol{b}\bullet\boldsymbol{e})(\boldsymbol{c}\bullet\boldsymbol{f})\boldsymbol{g}$ (see [20] for more details). Finally, the norm of a tensor $\boldsymbol{A}\in\mathrm{GT}(2)$ is defined with the help of the former contracted product according to $\|\boldsymbol{A}\|\equiv(\boldsymbol{A}:\boldsymbol{A})^{1/2}$.

2. Review of the bifurcation equations

We consider a very long cylindrical body as seen on the right-hand side in Fig. 2. By invoking the plane-strain approximation we shall confine our attention to a generic annular cross-section of inner radius R_1 and outer radius R_2, situated far away from the ends of the cylinder. Our main interest in what follows is with the possible in-plane bifurcations experienced by such a cross-section when the two curved boundaries are subjected to purely radial tensile loads.

All pre-bifurcation fields will be indicated by using "$\circ$" and the relevant bifurcation equations are derived from the method of adjacent equilibrium. For short, in our particular context this amounts to writing the equilibrium equations on two neighbouring stressed configurations and subtracting them, followed by a geometrical linearisation of the kinematics; the incremental displacement field between these two adjacent configurations will be referred to as $\boldsymbol{u}$.

In terms of the Piola–Kirchhoff (PK) tensors, the stresses in the two configurations can be represented as

$$\mathring{\boldsymbol{S}}=\mathring{\boldsymbol{\Pi}}\cdot(\boldsymbol{I}+\mathring{\boldsymbol{H}}^{\mathrm{T}})\quad\text{and}\quad\mathring{\boldsymbol{S}}+\boldsymbol{S}=(\boldsymbol{\Pi}+\mathring{\boldsymbol{\Pi}})\cdot(\boldsymbol{I}+\mathring{\boldsymbol{H}}^{\mathrm{T}}+\boldsymbol{H}^{\mathrm{T}}),$$

where $\boldsymbol{S}$ and $\boldsymbol{\Pi}$ denote the first and, respectively, the second PK tensors in the neutrally stable configuration, $\boldsymbol{H}=\boldsymbol{u}\otimes\boldsymbol{\nabla}$ is the displacement gradient in the same configuration, and $\boldsymbol{I}$ is the second-order identity tensor. By subtraction of these two relations it is found that

$$\boldsymbol{S}=\mathring{\boldsymbol{\Pi}}\cdot\boldsymbol{H}^{\mathrm{T}}+\boldsymbol{\Pi}\cdot(\boldsymbol{I}+\mathring{\boldsymbol{H}}^{\mathrm{T}}).\tag{1}$$

Next, we shall assume that the material satisfies a constitutive law of St. Venant–Kirchhoff type, i.e.

$$\boldsymbol{\Pi}=2\mu\boldsymbol{E}+\lambda|\boldsymbol{E}|\boldsymbol{I},\tag{2}$$

where $\boldsymbol{E}=(\boldsymbol{F}^{\mathrm{T}}\cdot\boldsymbol{F}-\boldsymbol{I})/2$ is the Lagrangian strain tensor, $\boldsymbol{F}=\boldsymbol{I}+\boldsymbol{u}\otimes\boldsymbol{\nabla}$ stands for the deformation gradient, $|\boldsymbol{E}|\equiv\boldsymbol{E}:\boldsymbol{I}$ represents its first principal invariant, and λ, μ denote the usual linear elastic constants. Note that, while geometrical non-linearities are allowed in the response function, material non-linearities are absent.

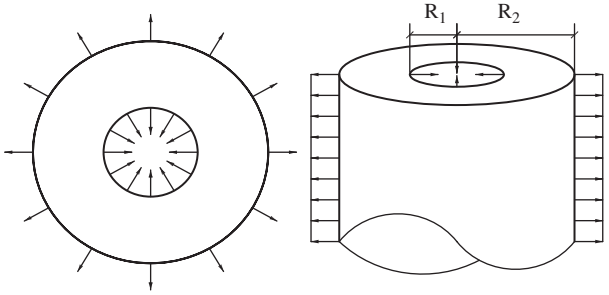

Fig. 2. A thick cylindrical body under radial tensile loads.

By writing (2) on the aforementioned two neighbouring configurations and following the same strategy that generated (1), we find

$$\begin{aligned}\boldsymbol{\Pi} &= \mu[(\mathring{\boldsymbol{H}}^{\mathrm{T}}+\boldsymbol{I})\cdot\boldsymbol{H}+\boldsymbol{H}^{\mathrm{T}}\cdot(\mathring{\boldsymbol{H}}+\boldsymbol{I})]+\lambda(|\boldsymbol{H}|+|\mathring{\boldsymbol{H}}^{\mathrm{T}}\cdot\boldsymbol{H}|)\boldsymbol{I}\\ &\simeq \mu(\boldsymbol{H}+\boldsymbol{H}^{\mathrm{T}})+\lambda|\boldsymbol{H}|\boldsymbol{I}.\end{aligned} \tag{3}$$

The expression of $\boldsymbol{S}$ in (1) can be further simplified by invoking a number of ad-hoc simplifications rehearsed by Novozhilov in [5]. To this end, we recall the decomposition into a symmetric and an anti-symmetric part for the displacement gradient, $\boldsymbol{H}=\boldsymbol{e}+\boldsymbol{\omega}$, with the first tensor describing changes in lengths, while the second characterises the rotation of material line elements according to

$$\boldsymbol{\omega}=\frac{1}{2}(\boldsymbol{u}\otimes\boldsymbol{\nabla}-\boldsymbol{\nabla}\otimes\boldsymbol{u}).$$

In Ref. [5] it is stipulated that

$$\|\boldsymbol{\Pi}\cdot\mathring{\boldsymbol{e}}\|,\quad \|\mathring{\boldsymbol{\Pi}}\cdot\boldsymbol{e}\|,\quad \|\boldsymbol{\Pi}\cdot\mathring{\boldsymbol{\omega}}\|\ll\|\mathring{\boldsymbol{\Pi}}\cdot\boldsymbol{\omega}\|,$$

which when used in conjunction with (1) leads to

$$\boldsymbol{S}\simeq\boldsymbol{\Pi}-\mathring{\boldsymbol{\Pi}}\cdot\boldsymbol{\omega}. \tag{4}$$

This can be substituted in the static equilibrium equation $\boldsymbol{\nabla}\cdot\boldsymbol{S}=\boldsymbol{0}$ to yield

$$\boldsymbol{\nabla}\cdot\boldsymbol{\Pi}-(\boldsymbol{\nabla}\cdot\mathring{\boldsymbol{\Pi}})\cdot\boldsymbol{\omega}-\mathring{\boldsymbol{\Pi}}:(\boldsymbol{\nabla}\otimes\boldsymbol{\omega})=\boldsymbol{0}.$$

If the pre-buckling deformation state is obtained within the framework of the classical linear theory of elasticity, the middle term in the above equation will be zero since $\boldsymbol{\Pi}\simeq\boldsymbol{S}\simeq\mathring{\boldsymbol{\sigma}}$, the last tensor in this sequence of approximations being the Cauchy stress. Furthermore, use of (2) will then allow us to cast the bifurcation equation in the following invariant form

$$\mu\nabla^2\boldsymbol{u}+(\lambda+\mu)\boldsymbol{\nabla}(\boldsymbol{\nabla}\bullet\boldsymbol{u})-\mathring{\boldsymbol{\sigma}}:(\boldsymbol{\nabla}\otimes\boldsymbol{\omega})=\boldsymbol{0}. \tag{5}$$

The boundary conditions associated with this equation are briefly reviewed below, but first we record an extension of it that involves the full expression of $\boldsymbol{\Pi}$ as given on the first line in (3),

$$\begin{aligned}&(\boldsymbol{\nabla}\otimes\boldsymbol{u}):\boldsymbol{Q}_1+(\boldsymbol{u}\otimes\boldsymbol{\nabla}):\boldsymbol{Q}_2+\boldsymbol{\nabla}\otimes(\boldsymbol{u}\otimes\boldsymbol{\nabla})\,\vdots\,\mathbb{L}_1+(\boldsymbol{u}\otimes\boldsymbol{\nabla})\otimes\boldsymbol{\nabla}\,\vdots\,\mathbb{L}_2\\ &+\boldsymbol{\nabla}\otimes(\boldsymbol{\nabla}\otimes\boldsymbol{u})\,\vdots\,\mathbb{L}_3+\boldsymbol{a}(\boldsymbol{\nabla}\bullet\boldsymbol{u})+(\nabla^2\boldsymbol{u})\cdot\boldsymbol{P}_1+\boldsymbol{\nabla}(\boldsymbol{\nabla}\bullet\boldsymbol{u})\cdot\boldsymbol{P}_2=\boldsymbol{0},\end{aligned} \tag{6}$$

where $\boldsymbol{a}\in\mathrm{GT}(1)$, $\boldsymbol{P}_j\in\mathrm{GT}(2)$, $\boldsymbol{Q}_j\in\mathrm{GT}(3)$ $(j=1,2)$, and $\mathbb{L}_j\in\mathrm{GT}(4)$ $(j=1,2,3)$ are defined by

$$\boldsymbol{a}\coloneqq\lambda(\nabla^2\mathring{\boldsymbol{u}}),$$

$$\boldsymbol{P}_1\coloneqq\mu(\boldsymbol{I}+\mathring{\boldsymbol{u}}\otimes\boldsymbol{\nabla})\cdot(\boldsymbol{I}+\boldsymbol{\nabla}\otimes\mathring{\boldsymbol{u}}),$$

$$\boldsymbol{P}_2\coloneqq(\lambda+\mu)(\boldsymbol{I}+\boldsymbol{\nabla}\otimes\mathring{\boldsymbol{u}}),$$

$$\begin{aligned}\boldsymbol{Q}_1\coloneqq{}&2\mu^t[(\mathring{\boldsymbol{u}}\otimes\boldsymbol{\nabla})+\boldsymbol{I}]\cdot(\boldsymbol{\nabla}\otimes(\boldsymbol{\nabla}\otimes\mathring{\boldsymbol{u}}))\\ &+\mu^t\{[(\boldsymbol{I}+\mathring{\boldsymbol{u}}\otimes\boldsymbol{\nabla})\cdot(\boldsymbol{I}\otimes\nabla^2\mathring{\boldsymbol{u}})+\boldsymbol{\nabla}\otimes(\boldsymbol{\nabla}\otimes\mathring{\boldsymbol{u}})]^t\},\end{aligned}$$

$$\boldsymbol{Q}_2\coloneqq\lambda(\mathring{\boldsymbol{u}}\otimes\boldsymbol{\nabla})\otimes(\nabla^2\mathring{\boldsymbol{u}})+\lambda((\mathring{\boldsymbol{u}}\otimes\boldsymbol{\nabla})\otimes\boldsymbol{\nabla})\cdot(\boldsymbol{I}+\boldsymbol{\nabla}\otimes\mathring{\boldsymbol{u}}),$$

$$\mathbb{L}_1\coloneqq\mu(\boldsymbol{\nabla}\otimes\mathring{\boldsymbol{u}})\otimes(\boldsymbol{I}+\boldsymbol{\nabla}\otimes\mathring{\boldsymbol{u}}),$$

$$\mathbb{L}_2\coloneqq\mu(\mathring{\boldsymbol{u}}\otimes\boldsymbol{\nabla})\otimes(\boldsymbol{I}+\boldsymbol{\nabla}\otimes\mathring{\boldsymbol{u}}),$$

$$\mathbb{L}_3\coloneqq\mathring{\boldsymbol{\sigma}}\otimes\boldsymbol{I}.$$

A quantitative comparison between the two Eqs. (5) and (6) has been carried out and will be reported elsewhere. (Despite the apparent complexity, in polar coordinates the coefficients of $\boldsymbol{\nabla}\otimes\boldsymbol{u}$, $\boldsymbol{\nabla}\otimes(\boldsymbol{u}\otimes\boldsymbol{\nabla})$, etc. in (6) take on relatively simple forms.)

Going now back to the derivation of the boundary constraints announced above, let $\widehat{\boldsymbol{n}}$ be the outward unit normal to the cylindrical surface of the original unstressed body, and let $\mathring{\boldsymbol{n}}$ and $\boldsymbol{n}$ be the normals to the prestressed and, respectively, the neutrally stable adjacent configurations. Thus, the traction boundary conditions can be written as

$$\mathring{\boldsymbol{S}}^T\cdot\widehat{\boldsymbol{n}}=\boldsymbol{t}(\mathring{\boldsymbol{u}})\quad\text{and}\quad(\mathring{\boldsymbol{S}}+\boldsymbol{S})^T\cdot\widehat{\boldsymbol{n}}=\boldsymbol{t}(\mathring{\boldsymbol{u}}+\boldsymbol{u}), \tag{7}$$

where $\boldsymbol{t}$ represents the given traction vector—possibly depending on the displacement field in the case of follower loads. In this situation $\boldsymbol{t}(\boldsymbol{u})=\sigma_j\boldsymbol{n}$, with $\sigma_j\in\mathbb{R}$ representing the magnitude of the applied radial stresses on $r=R_j$ $(j=1,2)$: $\sigma_j<0$ for compressive loads, while $\sigma_j>0$ in the tensile case.

Since we are interested in the case of small pre-buckling deformations, we can introduce the approximation $\widehat{\boldsymbol{n}}\simeq\mathring{\boldsymbol{n}}$ and then, with the help of (4), the difference of the two relations in (7) leads to

$$(\boldsymbol{\Pi}+\boldsymbol{\omega}\cdot\mathring{\boldsymbol{\Pi}})\cdot\mathring{\boldsymbol{n}}=\sigma_j(\boldsymbol{n}-\mathring{\boldsymbol{n}}). \tag{8}$$

On the other hand, Nanson's formula with $J\equiv\det\boldsymbol{F}\simeq1$ gives $\boldsymbol{n}\,\mathrm{d}a=\boldsymbol{F}^{-\mathrm{T}}\cdot\mathring{\boldsymbol{n}}\,\mathrm{d}\mathring{a}$, which on squaring out both sides produces

$$\begin{aligned}(\mathrm{d}a)^2&=\mathring{\boldsymbol{n}}\bullet\boldsymbol{F}^{-1}\cdot\boldsymbol{F}^{-\mathrm{T}}\cdot\mathring{\boldsymbol{n}}(\mathrm{d}\mathring{a})^2=\mathring{\boldsymbol{n}}\bullet[(\boldsymbol{I}+\boldsymbol{H})^{-1}\cdot(\boldsymbol{I}+\boldsymbol{H})^{-\mathrm{T}}\cdot\mathring{\boldsymbol{n}}](\mathrm{d}\mathring{a})^2\\ &\simeq(1-2\mathring{\boldsymbol{n}}\bullet(\boldsymbol{H}\cdot\mathring{\boldsymbol{n}}))(\mathrm{d}\mathring{a})^2,\end{aligned}$$

and hence

$$\boldsymbol{n}\simeq\boldsymbol{F}^{-\mathrm{T}}\cdot\mathring{\boldsymbol{n}}(1+\mathring{\boldsymbol{n}}\bullet(\boldsymbol{H}\cdot\mathring{\boldsymbol{n}})).$$

When used in conjunction with (8) this last equation yields

$$\sigma_j(\boldsymbol{n}-\mathring{\boldsymbol{n}})\simeq-\sigma_j\boldsymbol{H}^{\mathrm{T}}\cdot\mathring{\boldsymbol{n}}\simeq\sigma_j\boldsymbol{\omega}\cdot\mathring{\boldsymbol{n}},$$

where in deriving the last result we have assumed that $\|\boldsymbol{e}\|\ll\|\boldsymbol{\omega}\|$. In conclusion, the constraints on the two curved boundaries of the annulus are

$$(\boldsymbol{\Pi}+\boldsymbol{\omega}\cdot\mathring{\boldsymbol{\Pi}})\cdot\mathring{\boldsymbol{n}}=\sigma_j\boldsymbol{\omega}\cdot\mathring{\boldsymbol{n}}\quad\text{for } r=R_j\quad(j=1,2). \tag{9}$$

The term on the right-hand side of (9) has its origin in the changes of the applied forces with the current configuration, so this term will be absent in the case of dead loading.

Our next task will be to write the invariant-form Eqs. (5) and (9) in component form in order to make them amenable to numerical calculations in the next sections. To this end, let $\{\boldsymbol{g}_1,\boldsymbol{g}_2,\boldsymbol{g}_3\}$ and $\{\boldsymbol{g}^1,\boldsymbol{g}^2,\boldsymbol{g}^3\}$ be a pair of reciprocal bases associated with the problem at hand; expressed in the latter basis, the contravariant components of the identity tensor are $g^{ij}=\boldsymbol{g}^i\bullet\boldsymbol{g}^j$. A simple calculation then reveals that

$$\begin{aligned}\mathring{\boldsymbol{\sigma}}:(\boldsymbol{\nabla}\otimes\boldsymbol{\omega})&=\frac{1}{2}\mathring{\boldsymbol{\sigma}}:[\boldsymbol{\nabla}\otimes(\boldsymbol{u}\otimes\boldsymbol{\nabla})-\boldsymbol{\nabla}\otimes(\boldsymbol{\nabla}\otimes\boldsymbol{u})]\\ &=\frac{1}{2}\mathring{\sigma}^{ij}(\nabla_i\nabla_j u_k-\nabla_i\nabla_k u_j)\boldsymbol{g}^k,\end{aligned}$$

where $\nabla_p u_q\equiv u_{q,p}-\Gamma^r_{pq}u_r$ denotes the covariant derivative of u_q with respect to the $\boldsymbol{g}_p$-coordinate and $\Gamma^r_{pq}\equiv\boldsymbol{g}^r\bullet\boldsymbol{g}_{p,q}$ are the well-known Christoffel symbols. Since in addition to this,

$$\boldsymbol{\nabla}(\boldsymbol{\nabla}\bullet\boldsymbol{u})=(g^{ij}\nabla_k\nabla_i u_j)\boldsymbol{g}^k\quad\text{and}\quad\nabla^2\boldsymbol{u}=(g^{ij}\nabla_i\nabla_j u_k)\boldsymbol{g}^k,$$

the desired component form of Eq. (5) assumes the expression

$$\left(\mu g^{ij}+\frac{1}{2}\mathring{\sigma}^{ij}\right)\nabla_i\nabla_j u_k+(\lambda+\mu)g^{ij}\nabla_k\nabla_i u_j-\frac{1}{2}\mathring{\sigma}^{ij}\nabla_i\nabla_k u_j=0. \tag{10}$$

In cylindrical polar coordinates we find two coupled second-order partial differential equations for the components of the in-plane displacement field $\boldsymbol{u}(r,\theta)=u_r(r,\theta)\boldsymbol{e}_r+u_\theta(r,\theta)\boldsymbol{e}_\theta$,

$$A_{11}\frac{\partial^2u_r}{\partial r^2}+A_{12}\frac{\partial^2u_\theta}{\partial\theta\partial r}+A_{13}\frac{\partial^2u_r}{\partial\theta^2}+A_{14}\frac{\partial u_r}{\partial r}+A_{15}\frac{\partial u_\theta}{\partial\theta}+A_{16}u_r=0, \tag{11a}$$

$$A_{21}\frac{\partial^2 u_\theta}{\partial r^2}+A_{22}\frac{\partial^2 u_r}{\partial\theta\partial r}+A_{23}\frac{\partial^2 u_\theta}{\partial\theta^2}+A_{24}\frac{\partial u_\theta}{\partial r}+A_{25}\frac{\partial u_r}{\partial\theta}+A_{26}u_\theta=0, \quad (11b)$$

where

$$A_{11}:=\lambda+2\mu, \quad A_{21}:=\mu+\frac{1}{2}\mathring{\sigma}_{rr},$$

$$A_{12}:=\frac{1}{r}\left(\lambda+\mu-\frac{1}{2}\mathring{\sigma}_{\theta\theta}\right), \quad A_{22}:=\frac{1}{r}\left(\lambda+\mu-\frac{1}{2}\mathring{\sigma}_{rr}\right),$$

$$A_{13}:=\frac{1}{r^2}\left(\mu+\frac{1}{2}\mathring{\sigma}_{\theta\theta}\right), \quad A_{23}:=\frac{\lambda+2\mu}{r^2},$$

$$A_{14}:=\frac{\lambda+2\mu}{r}, \quad A_{24}:=\frac{1}{r}\left(\mu+\frac{1}{2}\mathring{\sigma}_{rr}\right),$$

$$A_{15}:=-\frac{1}{r^2}\left(\lambda+3\mu+\frac{1}{2}\mathring{\sigma}_{\theta\theta}\right), \quad A_{25}:=\frac{1}{r^2}\left(\lambda+3\mu+\frac{1}{2}\mathring{\sigma}_{rr}\right),$$

$$A_{16}:=-\frac{\lambda+2\mu}{r^2}, \quad A_{26}:=-\frac{1}{r^2}\left(\mu+\frac{1}{2}\mathring{\sigma}_{rr}\right).$$

Note that due to the plane-strain assumption the other equation obtained from (10) is automatically satisfied.

These equations are solved subject to the following boundary conditions at $r=R_j$ $(j=1,2)$,

$$B_{11}\frac{\partial u_r}{\partial r}+B_{12}\frac{u_\theta}{\partial\theta}+B_{13}u_r=0, \quad (12a)$$

$$B_{21}\frac{\partial u_r}{\partial\theta}+B_{22}\frac{\partial u_\theta}{\partial r}+B_{23}u_\theta=0, \quad (12b)$$

where the coefficients that appear above are given by

$$B_{11}:=\lambda+2\mu, \quad B_{21}:=\frac{1}{2r}[2\mu-(\mathring{\sigma}_{rr}-\sigma_j)],$$

$$B_{12}:=\frac{\lambda}{r}, \quad B_{22}:=\frac{1}{2}[2\mu+(\mathring{\sigma}_{rr}-\sigma_j)],$$

$$B_{13}:=\frac{\lambda}{r}, \quad B_{23}:=\frac{1}{2r}[-2\mu+(\mathring{\sigma}_{rr}-\sigma_j)].$$

The solution of the rather complicated system (11) and (12) is sought by using functions with separable variables, i.e.

$$u_r(r,\theta)=U_1(r)\cos n\theta \quad \text{and} \quad u_\theta(r,\theta)=U_2(r)\sin n\theta, \quad (13)$$

where the arbitrary integer $n\geq 0$ will be determined from the usual minimisation strategy employed in similar contexts (see, for instance, [15,16] for details on related problems). The amplitudes U_1 and U_2 turn out to satisfy two coupled second-order ordinary differential equations whose explicit expression we find next.

In the case of an elastic annulus loaded by radial tractions on both circular boundaries, the pre-buckling stress field has the well-known expression (e.g., see [19])

$$\mathring{\sigma}_{rr}=\sigma_2\left(A+\frac{B}{\rho^2}\right), \quad \mathring{\sigma}_{\theta\theta}=\sigma_2\left(A-\frac{B}{\rho^2}\right),$$

with

$$A:=\frac{\eta^2-\Lambda}{\eta^2-1}, \quad B:=\frac{\eta^2(\Lambda-1)}{\eta^2-1},$$

and

$$\rho:=\frac{r}{R_1}, \quad \eta:=\frac{R_2}{R_1}, \quad \Lambda:=\frac{\sigma_1}{\sigma_2}.$$

It can be shown that the hoop stresses will vanish along the circumference of the circle $\rho=\overline{\rho}$,

$$\overline{\rho}:=\left\{\frac{\eta^2(\Lambda-1)}{\eta^2-\Lambda}\right\}^{1/2},$$

furthermore, by letting

$$\Lambda_{\text{low}}=\frac{2\eta^2}{1+\eta^2}, \quad \Lambda_{\text{up}}=\frac{1}{2}(1+\eta^2),$$

we infer that if $\Lambda_{\text{low}}<\Lambda<\Lambda_{\text{up}}$ then the region $1<\rho<\overline{\rho}$ experiences azimuthal compression, while the remaining part of the annulus, $\overline{\rho}<\rho<\eta$, is in tension. Thus, we expect the possible bifurcations present in this problem to have a local character and to be confined near the inner rim of the annulus. In this respect the situation appears to be entirely analogous to that involving the plane-stress problems discussed in [15,16] but, as we shall see shortly, this is where the analogy stops.

After substituting the assumed form of solution (13) into the original Eqs. (11) and (12), the resulting boundary-value problem for the U_j's $(j=1,2)$ can be non-dimensionalised by introducing

$$\alpha:=\frac{\sigma_2}{E}, \quad \widehat{U}_1:=\frac{U_1}{R_2}, \quad \widehat{U}_2:=\frac{U_2}{R_2}.$$

Dropping the "hats" for notational convenience and denoting by a dash differentiation with respect to ρ, we record below the final form of the bifurcation equations that hold for $1<\rho<\eta$

$$\overline{A}_{11}U''_1+\overline{A}_{12}U'_2+(\overline{A}_{13}+\overline{A}_{16})U_1+\overline{A}_{14}U'_1+\overline{A}_{15}U_2=0, \quad (14a)$$

$$\overline{A}_{21}U''_2+\overline{A}_{22}U'_1+(\overline{A}_{23}+\overline{A}_{26})U_2+\overline{A}_{24}U'_2+\overline{A}_{25}U_1=0, \quad (14b)$$

where

$$\overline{A}_{11}:=K_1, \quad \overline{A}_{21}:=\frac{1}{2}\left[K_3+\alpha\left(A+\frac{B}{\rho^2}\right)\right],$$

$$\overline{A}_{12}:=\frac{n}{2\rho}\left[K_2-\alpha\left(A-\frac{B}{\rho^2}\right)\right], \quad \overline{A}_{22}:=-\frac{n}{2\rho}\left[K_2-\alpha\left(A+\frac{B}{\rho^2}\right)\right],$$

$$\overline{A}_{13}:=-\frac{n^2}{2\rho^2}\left[K_3+\alpha\left(A-\frac{B}{\rho^2}\right)\right], \quad \overline{A}_{23}:=-\frac{n^2K_1}{\rho^2},$$

$$\overline{A}_{14}:=\frac{K_1}{\rho}, \quad \overline{A}_{24}:=\frac{1}{2\rho}\left[K_3+\alpha\left(A+\frac{B}{\rho^2}\right)\right],$$

$$\overline{A}_{15}:=-\frac{n}{2\rho^2}\left[K_4+\alpha\left(A-\frac{B}{\rho^2}\right)\right], \quad \overline{A}_{25}:=-\frac{n}{2\rho^2}\left[K_4+\alpha\left(A+\frac{B}{\rho^2}\right)\right],$$

$$\overline{A}_{16}:=-\frac{K_1}{\rho^2}, \quad \overline{A}_{26}:=-\frac{1}{2\rho^2}\left[K_3+\alpha\left(A+\frac{B}{\rho^2}\right)\right],$$

and

$$K_1=\frac{1-\nu}{(1+\nu)(1-2\nu)}, \quad K_2=\frac{1}{(1+\nu)(1-2\nu)},$$

$$K_3=\frac{1}{1+\nu}, \quad K_4=\frac{3-4\nu}{(1+\nu)(1-2\nu)}, \quad K_5=\nu K_2.$$

The (relatively small) parameter α that enters in these equations will be regarded as fixed in the numerical simulations of the next section.

The rescaled boundary conditions can be written in condensed form as

$$\overline{B}^{(j)}_{11}U'_1+\overline{B}^{(j)}_{12}U_2+\overline{B}^{(j)}_{13}U_1=0, \quad (15a)$$

$$\overline{B}^{(j)}_{21}U'_2+\overline{B}^{(j)}_{22}U_2+\overline{B}^{(j)}_{23}U_1=0, \quad (j=1,2), \quad (15b)$$

where the case $j=1$ corresponds to the inner rim $(\rho=1)$, and $j=2$ applies to the outer boundary $(\rho=\eta)$. The expressions of the above coefficients take on different forms in the case of dead and follower loads, but can be written compactly as

$$B^{(1)}_{11}=K_1, \quad B^{(1)}_{21}=\frac{1}{2}[K_3+\alpha(A+B)-\underline{\underline{\alpha}}],$$

$$B_{12}^{(1)} = nK_5, \quad B_{22}^{(1)} = \frac{1}{2}[-K_3 + \alpha(A+B) - \underline{\alpha}],$$

$$B_{13}^{(1)} = K_5, \quad B_{23}^{(1)} = -\frac{n}{2}[K_3 - \alpha(A+B) + \underline{\alpha}],$$

and

$$B_{11}^{(2)} = K_1, \quad B_{21}^{(2)} = \frac{1}{2}\left[K_3 + \alpha\left(A + \frac{B}{\eta^2}\right) - \underline{\underline{\alpha\lambda}}\right],$$

$$B_{12}^{(2)} = \frac{nK_5}{\eta}, \quad B_{22}^{(2)} = \frac{1}{2\eta}\left[-K_3 + \alpha\left(A + \frac{B}{\eta^2}\right) - \underline{\underline{\alpha\lambda}}\right],$$

$$B_{13}^{(2)} = \frac{K_5}{\eta}, \quad B_{23}^{(2)} = -\frac{n}{2\eta}\left[K_3 - \alpha\left(A + \frac{B}{\eta^2}\right) + \underline{\underline{\alpha\lambda}}\right],$$

with the caveat that the underlined terms do not appear in the case of dead loading, whereas for follower loads all the $\alpha-$terms in the square brackets must be omitted (see also the remarks made after Eq. (9)). We mention in passing that the equations set up in this section are equivalent to the ones in [7]—cf. (27) and (28) featuring in that reference.

3. Numerical results

Direct numerical simulations of the boundary-value problem (14) and (15) were carried out in the usual fashion by first rewriting the equations as a first-order four-by-four linear system, which was then tackled with the help of the compound matrix method [15,16]. In using the separable variable solutions (13) it was tacitly assumed that the Eqs. (11) were elliptic. However, owing to the presence of variable coefficients, this statement need not be true everywhere in the annulus and, in fact, the equations do lose ellipticity for sufficiently large values of Λ. Also, since we are essentially concerned with a traction boundary-value problem, another subtle point is the verification of the Shapiro–Lopatinskij condition (SLC). In order to understand the range of validity for the numerical integration of the ordinary differential equations, we first examine briefly under what conditions the loss of ellipticity becomes possible, and later we comment on the SLC.

To this end let us observe that (11) can be arranged in the form

$$\mathcal{L}_{rr}[u_r] + \mathcal{L}_{r\theta}[u_\theta] = 0, \tag{16a}$$

$$\mathcal{L}_{\theta r}[u_r] + \mathcal{L}_{\theta\theta}[u_\theta] = 0, \tag{16b}$$

where the differential operators that appear above have the following definitions,

$$\mathcal{L}_{rr} \equiv A_{11}\frac{\partial^2}{\partial r^2} + A_{13}\frac{\partial^2}{\partial\theta^2} + A_{14}\frac{\partial}{\partial r} + A_{16},$$

$$\mathcal{L}_{r\theta} \equiv A_{12}\frac{\partial^2}{\partial r\partial\theta} + A_{15}\frac{\partial}{\partial\theta},$$

$$\mathcal{L}_{\theta r} \equiv A_{22}\frac{\partial^2}{\partial r\partial\theta} + A_{25}\frac{\partial}{\partial\theta},$$

$$\mathcal{L}_{\theta\theta} \equiv A_{21}\frac{\partial^2}{\partial r^2} + A_{23}\frac{\partial^2}{\partial\theta^2} + A_{24}\frac{\partial}{\partial r} + A_{26}.$$

The principal part of the symbol associated with the system (16) is defined by (see [21], for example)

$$\mathbf{L}^p(\boldsymbol{x}, \mathrm{i}\boldsymbol{\xi}) := -\begin{bmatrix} A_{11}(\boldsymbol{x})\xi_1^2 + A_{13}(\boldsymbol{x})\xi_2^2 & A_{12}(\boldsymbol{x})\xi_1\xi_2 \\ A_{22}(\boldsymbol{x})\xi_1\xi_2 & A_{21}(\boldsymbol{x})\xi_1^2 + A_{23}(\boldsymbol{x})\xi_2^2 \end{bmatrix}, \quad (\mathrm{i} = \sqrt{-1}), \tag{17}$$

where $\boldsymbol{\xi} \equiv (\xi_1, \xi_2) \in \mathbb{R}^2$ and we have indicated explicitly the dependence of the coefficients A_{ij} on the independent variable $\boldsymbol{x} \equiv (r, \theta)$. The type of the partial differential system (16) is classified according to the behaviour of $\mathbf{L}^p$, regarded as a quadratic form in ξ_1 and ξ_2. In particular, ellipticity requires that

$$\det \mathbf{L}^p(\boldsymbol{x}, \mathrm{i}\boldsymbol{\xi}) \neq 0, \quad (\forall)\boldsymbol{\xi} \in \mathbb{R}^2,$$

which after setting $t := \xi_2/\xi_1$, $(\xi_1 \neq 0)$, can be reduced to the study of the signs of the roots for the bi-quadratic

$$Z_3 + Z_2 t^2 + Z_1 t^4 = 0, \tag{18}$$

where

$$Z_1 := A_{11}A_{21},$$

$$Z_2 := A_{11}A_{23} + A_{13}A_{21} - A_{22}A_{12},$$

$$Z_3 := A_{13}A_{23}.$$

This can be further transformed into a quadratic by making the obvious substitution $s = t^2$; if the equation in s has either negative or complex conjugate roots, then the problem is elliptic. Loss of ellipticity will occur when one of the roots passes through zero. Note also that due to the axial symmetry of the coefficients A_{ij} in (11), the boundary curve separating the elliptic regions of the material from the non-elliptic ones will have to be some circle $\rho = \text{const}$.

The discriminant of the quadratic in s is always positive as it turns out to be equal to

$$\left[\frac{1}{2r^2}(\lambda + 2\mu)(\mathring{\sigma}_{rr} - \mathring{\sigma}_{\theta\theta})\right]^2,$$

and the sum of the roots of the quadratic is proportional to $\mathring{\sigma}_{rr} + \mathring{\sigma}_{\theta\theta} - 4\mu$. Since $2/3 < K_3 < 1$ and α is a relatively small parameter, it transpires that the sum of the roots is always negative. Thus, the condition for the loss of ellipticity will be given by $Z_3 = 0$ (since $Z_1 > 0$, after some routine calculations), with the result that

$$\Lambda = \frac{\rho^2[\eta^2 + (K_3/\alpha)(\eta^2 - 1)] + \eta^2}{\rho^2 + \eta^2}. \tag{19}$$

Regarded as a function of ρ, while all the other parameters are being kept fixed, $\Lambda = \Lambda(\rho)$ is an increasing function—as can be checked immediately by computing the derivative $\Lambda'(\rho)$. This means that loss of ellipticity will first occur for $\rho = 1$, i.e. at the inner rim. In conclusion, the curve that gives the loss of ellipticity in the $\Lambda - \eta$ plane, say $\mathcal{C}$, has a simple analytical expression,

$$(\mathcal{C}): \quad \Lambda_{\mathrm{ep}} = \frac{2\eta^2}{\eta^2 + 1} + \frac{K_3}{\alpha}\left(\frac{\eta^2 - 1}{\eta^2 + 1}\right). \tag{20}$$

If $0 < \Lambda < \Lambda_{\mathrm{ep}}$ then the system (16) is elliptic and this is precisely the regime of interest here; note that the first term on the right-hand side of (20) is just Λ_{low} defined in the previous section.

It can be seen that the principal part of the symbol associated with the more complicated Eq. (6) does not coincide with (17) because the inhomogeneous character of the pre-bifurcation state of stress. This makes the analysis of that new equation even more relevant to understanding the nature of the simplifications that led to (5) and the potential loss of ellipticity. While for a homogeneous basic state both (5) and (6) are justly expected to produce very similar outcomes, it does not appear sensible to maintain these expectations in the case dealt with here.

The first set of numerical results appears recorded in Fig. 3 and applies to the case of follower loads. We show the neutral stability curves corresponding to (14) and (15) for an increasing sequence of mode numbers ranging between 2 and 1000, when $\alpha = 0.05$ and $\nu = 0.33$. Changing these parameters does alter the *quantitative* features of the results, but the overall qualitative picture remains the same. Superimposed on these plots, the curve $\mathcal{C}$ is shown as the thick dashed line. It can be seen that the mode number $n = 2$ leads to the lowest eigenvalue for annular widths of up to $\eta \simeq 5.0$. Beyond

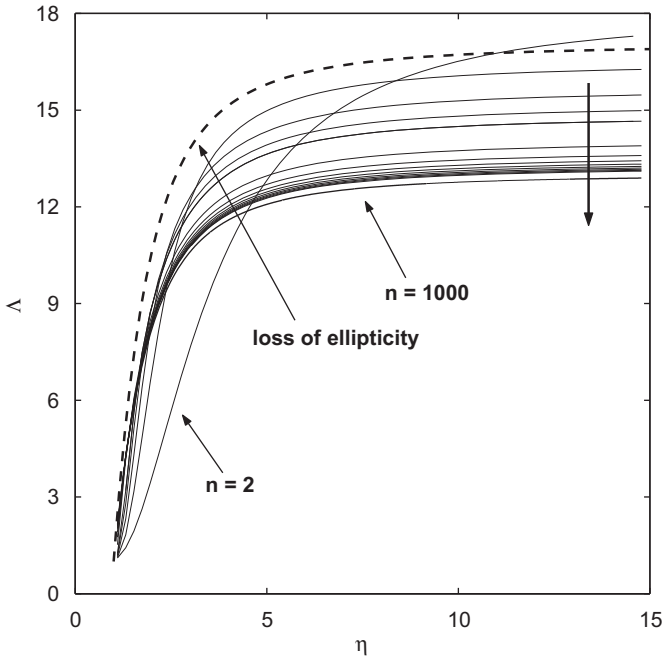

Fig. 3. Dependence of the eigenvalues Λ on the aspect ratio $\eta > 1$ for different mode numbers: $n = 2,4,\ldots,8,10,20,\ldots,80,100,1000$ in the case of *follower loads*. The thick arrow indicates the direction of increasing n and the dashed curve represents the loss of ellipticity boundary, as given by Eq. (20). Here $\alpha = 0.05$ and $\nu = 0.33$.

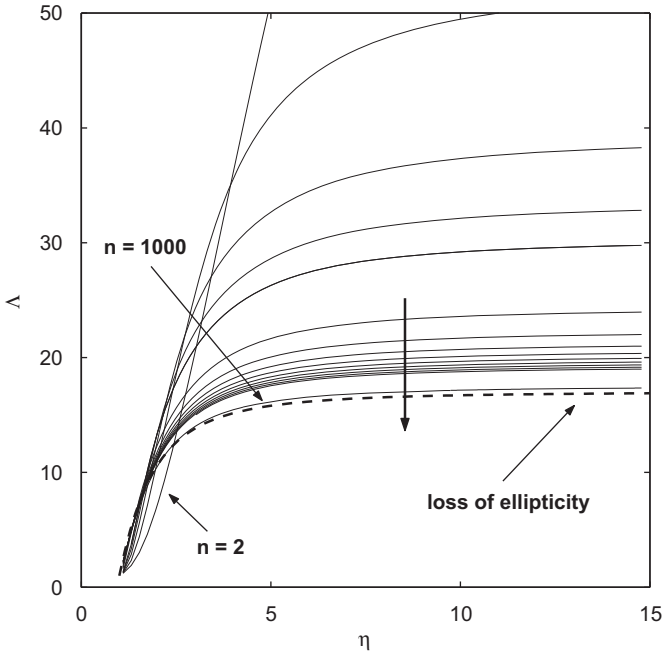

Fig. 4. Response curves similar to Fig. 3, but in the case of *dead loading*; all values of the parameters are the same as before and the thick arrow shows again the direction of increasing mode numbers.

that critical value, as n increases, the neutral stability curves move progressively into the elliptic region and seem to converge towards a limiting curve, which hereafter will be identified as $\mathcal{C}_\infty$. While not entirely obvious at this stage, the critical values of Λ associated with this curve involve a form of material rather than kinematic instability. In the next section we are going to show how an analytical approximation of $\mathcal{C}_\infty$ can be obtained by invoking some basic singular-perturbation arguments. In conclusion, when follower loads are considered the critical mode numbers are either $n=2$ or ∞; the latter is essentially a material instability and is associated with the failure of the SLC—hence, the curve $\mathcal{C}_\infty$ provides the boundary in the $\Lambda-\eta$ plane across which this condition is violated.

When dead (or rigid) loading is considered we have included a typical scenario in Fig. 4, which is laid out in the same fashion as the previous Figure. Note that the loss-of-ellipticity boundary $\mathcal{C}$ appears now as the envelope of the neutral stability curves as $n\to\infty$. For smallish values of η (up to approximately 2.0), all response curves are inside the elliptic region and the lowest eigenvalue is rendered by $n=2$, just as before. However, increasing the width of the annular domain, these curves are then found above the curve $\mathcal{C}$, which this time is attained in the limit of (infinitely) large mode numbers (i.e. $\mathcal{C}\simeq\mathcal{C}_\infty$, at least for largish η's). We recall here the well-known fact that the loss of ellipticity is a property of the differential equations themselves and it is independent of the type of boundary conditions employed. So in both Figs. 3 and 4 the dashed line is the same, what changes is the position and the topology of the neutral stability curves. From this perspective the results obtained are to be expected, although the sharp transition between the two instability modes in Fig. 3 cannot be anticipated right from the outset.

For the sake of completeness in Fig. 5 we illustrate the eigenmodes for $n\to\infty$ in the case of follower loads. It is immediately clear that as n grows, i.e. the spatial oscillations in the azimuthal direction increase, the amplitude functions U_1 and U_2 defined in (13) get closer and closer to the inner rim of the annular domain. We mention in passing that these functions also display localisation if n is kept fixed and $\eta\to\infty$.

4. The limit $n \gg 1$

While in principle it would be possible to carry out an asymptotic analysis of (14) subject to either follower or dead loads, it is only the former case that is of some theoretical interest, and which, therefore, deserves a closer scrutiny. For the sake of completeness, we shall also make a few remarks regarding the asymptotic structure of the problem for dead loads. As it will become clear from our asymptotic calculations, the leading-order analysis presented here is in fact directly relevant to establishing the limits of validity for the SLC—although in keeping with the informal style of the paper we shall not stress the technical side of that aspect. Section 5 of Ref. [22] contains some pertinent comments about similar situations and the ramifications to non-linear bifurcation problems.

To begin, in the limit $n\gg 1$ we introduce the stretched variable $X=\mathcal{O}(1)$ such that $\rho = 1+Xn^{-1}$, and look for solutions of (14) with

$$\boldsymbol{U} = \boldsymbol{U}_0(X)+\boldsymbol{U}_1(X)\frac{1}{n}+\cdots, \tag{21a}$$

$$\Lambda = \Lambda_0+\frac{\Lambda_1}{n}+\cdots, \tag{21b}$$

where

$$\boldsymbol{U} \coloneqq \begin{bmatrix} U_1 \\ U_2 \end{bmatrix}, \quad \boldsymbol{U}_j(X) \coloneqq \begin{bmatrix} U_{1j}(X) \\ U_{2j}(X) \end{bmatrix} \quad (j=0,1,\ldots).$$

The quantities that appear on the right-hand sides of (21) can be found systematically, although for our immediate purposes a leading-order analysis will suffice.

Routine algebraic manipulations indicate that if $\eta=\mathcal{O}(1)$ the boundary-layer behaviour is described by a hierarchy of equations governed by the differential operator

$$\mathcal{L}_{\mathrm{BL}} \equiv \boldsymbol{M}^{(2)}\frac{d^2}{dX^2}+\boldsymbol{M}^{(1)}\frac{d}{dX}+\boldsymbol{M}^{(0)}, \tag{22}$$

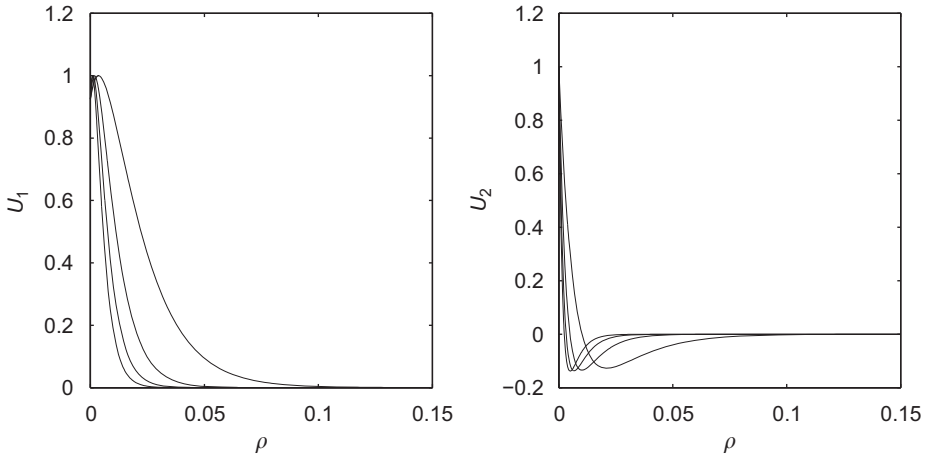

Fig. 5. Normalised eigenmodes of (14a) for follower loading when $\alpha=0.05$, $\nu=0.33$, and $\eta=5.0$. Both U_1 and U_2 undergo localisation as the mode number n is progressively increased; here, $n=50$, 100, 150, 200. The independent variable $1.0\le\rho\le 5.0$ has been suitably adjusted to a smaller range in order to enhance the clarity of the localisation process.

where the matrices $\boldsymbol{M}^{(j)}\in\mathcal{M}_{2\times 2}(\mathbb{R})$ have the components recorded below

$$M_{11}^{(2)}:=K_1,\quad M_{11}^{(1)}:=0,$$

$$M_{12}^{(2)}:=0,\quad M_{12}^{(1)}:=\frac{\alpha}{2(\eta^2-1)}[\Lambda_0(\eta^2+1)-2\eta^2]+\frac{K_2}{2},$$

$$M_{21}^{(2)}:=0,\quad M_{21}^{(1)}:=-\frac{1}{2}(K_2-\alpha\Lambda_0),$$

$$M_{22}^{(2)}:=\frac{1}{2}(K_3+\alpha\Lambda_0),\quad M_{22}^{(1)}:=0,$$

$$M_{11}^{(0)}:=\frac{\alpha}{2(\eta^2-1)}[\Lambda_0(\eta^2+1)-2\eta^2]-\frac{K_3}{2},$$

$$M_{12}^{(0)}:=0,$$

$$M_{21}^{(0)}:=0,$$

$$M_{22}^{(0)}:=-K_1.$$

The leading-order terms in (21) satisfy

$$\mathcal{L}_{\mathrm{BL}}[\boldsymbol{U}_0]=\boldsymbol{0};\tag{23}$$

when dead loads are considered, this equation must be solved subject to the homogeneous boundary conditions

$$\boldsymbol{H}^{(1)}\frac{d\boldsymbol{U}_0}{dX}+\boldsymbol{H}^{(0)}\boldsymbol{U}_0=\boldsymbol{0}\quad\text{at } X=0,\tag{24}$$

where

$$\boldsymbol{H}^{(1)}:=\begin{bmatrix}K_1 & 0\\ 0 & \alpha\Lambda_0+K_3\end{bmatrix}\quad\text{and}\quad\boldsymbol{H}^{(0)}:=\begin{bmatrix}0 & K_5\\ \alpha\Lambda_0-K_3 & 0\end{bmatrix}.$$

These constraints apply to follower loads as well, with the only modification that the parameter α in $\boldsymbol{H}^{(0)}$ and $\boldsymbol{H}^{(1)}$ must be set equal to zero. In both cases a second set of constraints must be enforced, as motivated by the numerical experiments of Section 3,

$$\frac{d^j\boldsymbol{U}_0}{dX^j}\to\boldsymbol{0}\quad\text{as } X\to\infty,\quad(j=0,1).\tag{25}$$

Looking for a solution of (23) in the form $\boldsymbol{U}_0(X)=\boldsymbol{v}\exp(\zeta X)$, for some $\zeta\in\mathbb{C}$ and a column vector $\boldsymbol{v}\in\mathbb{R}^2$, it is found that the former must satisfy the characteristic equation

$$\det[\zeta^2\boldsymbol{M}^{(2)}+\zeta\boldsymbol{M}^{(1)}+\boldsymbol{M}^{(0)}]=0,$$

with the roots

$$\zeta_{1,2}=\pm 1\quad\text{and}\quad\zeta_{3,4}=\pm\beta(\Lambda_0,\eta),\tag{26}$$

where

$$\beta(\Lambda_0,\eta):=\sqrt{\frac{K_3-2G}{K_3+\alpha\Lambda_0}},\quad G:=\frac{\alpha}{2(\eta^2-1)}[\Lambda_0(\eta^2+1)-2\eta^2].\tag{27}$$

Guided by the fact that the requirement (25) must hold in the far-field, the boundary-layer solution must be a linear combination of two exponentials involving the negative values from (26). Substituting this function in the two boundary conditions (24) results in the determinantal equation that supplies Λ_0. In the case of follower loads it is found that

$$H_3\Lambda_0^3+H_2\Lambda_0^2+H_1\Lambda_0+H_0=0,\tag{28}$$

where

$$H_0=-\frac{H_{04}\eta^4+H_{02}\eta^2+H_{00}}{(\eta^2-1)^2(\nu+1)^3},\quad H_1=-\frac{\alpha(H_{14}\eta^4+H_{12}\eta^2+H_{10})}{(\eta^2-1)^2(\nu+1)^2},$$

$$H_2=\frac{\alpha^2(H_{24}\eta^4+H_{22}\eta^2+H_{20})}{(\eta^2-1)^2(\nu+1)},\quad H_3=-\frac{\alpha^3(H_{34}\eta^4+H_{32}\eta^2+H_{30})}{(\eta^2-1)^2},$$

and

$$H_{04}:=4\alpha^2(1-\nu^2)^2-2\alpha(1+\nu)-1,\quad H_{02}:=2[\alpha(\nu+1)+1],$$

$$H_{14}:=4\alpha^2(1-\nu^2)^2-4\alpha(\nu^3+1)+1-2\nu,$$
$$H_{12}:=4[\alpha(-\nu^3+2\nu^2+2\nu-1)+\nu],$$

$$H_{24}:=4\alpha(1-\nu)-2\alpha\nu^2(1-3\nu)-1,$$
$$H_{22}:=2[\alpha\nu^2(\nu-3)+2\nu(1-\nu)+2\alpha(1-\nu)-1],$$

$$H_{34}:=2\nu^2-2\nu+1,\quad H_{32}:=2(\nu-1)^2,$$

$$H_{00}:=-1,\quad H_{10}:=-(1+2\nu),\quad H_{20}:=4\nu-1,\quad H_{30}:=1-2\nu.$$

The results predicted by (28) are compared in Fig. 6 with the direct numerical simulations of (14) and (15) for $n=1000$ (which could serve as a good approximation for $\mathcal{C}_\infty$). For the sake of brevity we show only a representative sample of calculations corresponding to $\nu=0.33$ and $\alpha=0.05/0.005$, because no qualitative differences are observed when changing these parameters. It is evident that the agreement is excellent and the leading-order ansatz (21) does capture all the features of the numerical solution.

If we try to approach the dead-loading problem with the same type of ansatz, then it quickly transpires that such a strategy

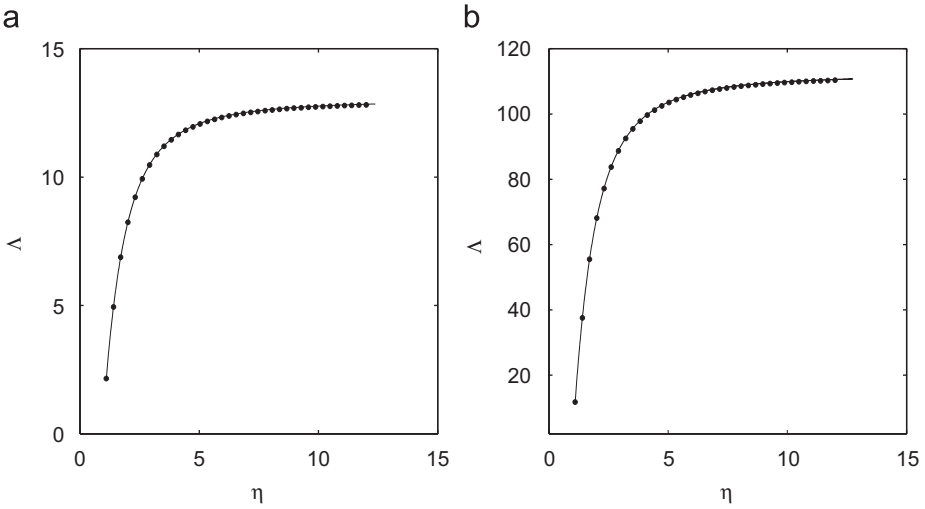

Fig. 6. Follower loads: comparisons between the limiting curves $\Lambda \equiv \Lambda_0(\eta)$ predicted by the leading-order determinantal equations (*dotted lines*) and their counterparts obtained from direct numerical simulations of (14) and (15) in the large-n limit (*continuous curves*, $n=1000$). In both windows $\nu = 0.33$, while $\alpha = 0.05$ in (a), and $\alpha = 0.005$ in (b).

would eventually be doomed for according to (27) as (Λ_0,η) gets close to the curve $\mathcal{C}$ defined in (20), $\beta(\Lambda_0,\eta)\to 0$. Hence there is now only one solution of (23) that falls off exponentially for $X\to\infty$. In this case the determinantal equation loses its relevance since it was obtained under the assumption that $\beta(\Lambda_0,\eta)=\mathcal{O}(1)$.

Fig. 4 shows clearly that the neutral stability curves tend to accumulate on $\mathcal{C}$ (the dashed curve) in the limit $n\gg 1$. Interestingly enough, this feature is anticipated by the old expansion (21) although, as we have just remarked above, this leads to some spurious results as well. Following the same strategy that led to (28), its counterpart in the dead loading case is

$$(K_3-2G)(E_2\Lambda_0^2+E_1\Lambda_0+E_0)=0, \tag{29}$$

with

$$E_2 := \frac{4\alpha^2(1-\nu)^2}{\eta^2-1}+\alpha^2(\eta^2+1),$$

$$E_1 := -2\alpha(\alpha\eta^2-K_3)-\frac{8\alpha^2\eta^2(1-\nu)^2}{\eta^2-1},$$

$$E_0 := \frac{4\alpha^2\eta^4(1-\nu)^2}{\eta^2-1}-K_3^2(\eta^2-1)-2K_3\alpha\eta^2.$$

Setting to zero the first bracket we get precisely the equation for the curve that marks the loss of ellipticity boundary in the $\Lambda-\eta$ plane. Alternatively, one can solve the quadratic in the second bracket that turns out to have a unique root $\Lambda_0>0$ slightly below that predicted by the previous equation. This apparent contradiction is a consequence of using the determinantal Eq. (29) beyond its intended range of validity. We have checked numerically for mode numbers up to $n=5\times 10^4$ that confirmed the accuracy of the scenario recorded in Fig. 4 (that is, the response curves approach the dashed curve from above).

To unravel the reason of the discrepancy generated by (29) we need to go back to the differential Eq. (14). When $K_3-2G=0$ it is easily checked that $\overline{A}_{13}(\rho=1)=0$ and (14) admits an $\mathcal{O}(n^{-2/3})$ boundary layer governed by a rescaled Airy function, with the eigenvalue expanding now in powers of $n^{-2/3}$. The $\mathcal{O}(n^{-1})$-layer still survives and it is possible to carry out a relatively standard analysis involving the interaction of the two layers, very much in the spirit of [15,16]. Since the non-elliptic regime is outwith the range of physical interest the details of that analysis are left out.

The boundary-value problem (14) and (15) contains a couple of additional parameters besides the mode number. Several asymptotic regimes can be investigated in this respect, for instance $0<\alpha\ll 1$ or $\eta\gg 1$ or assuming that the relative order of magnitude of these parameters are related to each other. However, none of these appears to be relevant to our immediate purposes, so we do not pursue matters further here.

5. Concluding remarks

We have considered the in-plane bifurcations of the classical plane-strain Lamé solutions for a St. Venant–Kirchhoff elastic solid. One of the main aims of this work has been to explore the applicability of the asymptotic strategy proposed in [11,14] to the case when the bifurcations are associated with a stressed rather than a free surface. Within the context of the simplified incremental deformation theory adopted here—SIDT (e.g., [1,5,6]), it was shown that this is indeed possible, but the outcome is somewhat different from that of the earlier investigations. In the scenario for the pure bending of a neo-Hookean rubber block discussed in [11] the transition between small and large mode numbers was gradual and depended intimately on the ratio of thickness to length. More exactly, the larger the width of the block, the greater the number of ripples on the compressed side. In the limit of an infinitely large block the critical principal stretch became equal to that found in the compression of a half-plane [3]. The problem was strongly elliptic and the instabilities found had a kinematic character. Here, perhaps because of the fact that both boundaries of the annulus are stressed, the neutrally stable configuration has less freedom in accommodating the full spectrum of mode numbers. Our results indicated that in the case of follower loads, for a small range of annulus widths, $\eta\simeq 1-2$ when $\alpha=0.05$ and $\nu=0.33$ ($\eta\equiv R_2/R_1$), the predominant long-wave deformation mode corresponds to the inner rim becoming an ellipse. For larger widths a short-wavelength (material) instability is observed whereby the central hole of the cylinder experiences fine warping; this wrinkling-type instability is directly linked to the failure of the Shapiro–Lopatinskij condition. In the case of dead loading loss of ellipticity dominates the global picture, although there is still a narrow window of annular widths for which the long-wave mode ($n=2$) persists. (These findings were robust when changing the Poisson's ratio $0<\nu<0.5$ and the non-dimensional parameter $\alpha\equiv\sigma_2/E$).

While from a practical point of view the immediate relevance of the specific type of loading adopted in this study is somewhat limited, the results reported here contribute towards a further rational understanding of the bifurcation phenomena experienced by elastic solids subjected to tensile loads. Our work also shows that one must tread with caution when dealing with incremental bifurcation equations involving non-homogeneous basic states because loss of ellipticity can severely restrict the scope of mathematical investigations. Last but not least, the work reported here reinforces the relevance of singular perturbation methods not only to thin-walled configurations, but also to incrementally linear elastic solids.

An immediate extension of this work vis-á-vis the developments of Section 3 could be directed towards the role of the boundary loading imposed on the annulus. For instance, the stress concentration phenomenon persists if the domain undergoes azimuthal shearing along the inner boundary, with tensile tractions still being imposed on the outer perimeter. By analogy with the plane-stress calculations carried out in [16] we expect the asymptotic structure of the problem to be different due to the obvious rotational symmetry inherent in that problem.

Finally, it is also of interest to understand whether the phenomena observed in this paper are an immediate consequence of the approximate nature of the SIDT; in this respect a comparison of the present analysis with a more rigorous one based on Ogden's incremental elasticity formulation would be desirable. We hope to return to this interesting issue in a forthcoming publication.

Acknowledgement

The second author was supported by a Studentship provided by the Engineering and Physical Sciences Research Council (UK) through Grant EP/F035136. He also thanks the University of Glasgow for additional financial aid.

References

[1] M.A. Biot, Mechanics of Incremental Deformation, John Wiley & Sons, New York, 1965.
[2] R.W. Ogden, Non-linear Elastic Deformations, Dover Publications, New York, 1997.
[3] M.A. Biot, Surface instability of rubber in compression, Applied Science Research A 12 (1963) 168–182.
[4] R. Hill, J.W. Hutchinson, Bifurcation phenomena in the plane tension test, Journal of the Mechanics and Physics of Solids 23 (1975) 239–264.
[5] V.V. Novozhilov, Foundations of the Nonlinear Theory of Elasticity, Dover Publications, New York, 1999.
[6] C.B. Biezeno, H. Hencky, On the general theory of elastic stability, Koninklijke Akademie van Wettenschappen te Amsterdam 31 (1928) 569–592.
[7] G.A. Kardomateas, Buckling of thick orthotropic cylindrical shells under external pressure, ASME Journal of Applied Mechanics 60 (1993) 195–202.
[8] G.A. Kardomateas, J. Simitses, Buckling of long sandwich cylindrical shells under external pressure, ASME Journal of Applied Mechanics 72 (2005) 493–500.
[9] N.D. Cristescu, E.M. Craciun, E. Soós, Mechanics of Elastic Composites, Chapman Hall/CRC Press, Boca Raton, 2004.
[10] G. Papadakis, Buckling of thick cylindrical shells under external pressure: a new analytical expression for the critical load and comparisons with elasticity solutions, International Journal of Solids and Structures 45 (2008) 5308–5321.
[11] C.D. Coman, M. Destrade, Asymptotic results for bifurcations in pure bending of rubber blocks, Quarterly Journal of Mechanics and Applied Mathematics 61 (2008) 395–414.
[12] A.N. Gent, I.S. Cho, Surface instabilities in compressed or bent rubber blocks, Rubber Chemistry and Technology 72 (1999) 253–262.
[13] R.S. Rivlin, Large elastic deformations of isotropic materials V: The problem of flexure, Proceedings of the Royal Society of London A 195 (1949) 463–473.
[14] C.D. Coman, Elastic instabilities caused by stress concentration, International Journal of Engineering Science 46 (2008) 877–890.
[15] C.D. Coman, A.P. Bassom, On the wrinkling of a pre-stressed annular thin film in tension, Journal of the Mechanics and Physics of Solids 55 (2007) 1601–1617.
[16] C.D. Coman, A.P. Bassom, Boundary layers and stress concentration in the circular shearing of annular thin films, Proceedings of the Royal Society of London A 463 (2007) 3037–3053.
[18] C.D. Coman, Boundary layers in incremental elasticity with application to the eversion of thick-walled tubes, Unpublished manuscript, 2008.
[19] P.C. Chou, N.J. Pagano, Elasticity: Tensor, Dyadic and Engineering Approaches, D. Van Nostrand Company, Princeton, 1967.
[20] D.C. Leigh, Nonlinear Continuum Mechanics, McGraw-Hill Book Company, New York, 1968.
[21] Y.V. Egorov, M.A. Shubin, Foundations of the Classical Theory of Partial Differential Equations, Springer Verlag, New York, 1998.
[22] P.V. Negron-Marrero, E. Montes-Pizarro, The complementary condition and its role in a bifurcation theory applicable to nonlinear elasticity, New York Journal of Mathematics 17a (2011) 1–21.